# The Numerical Solution of Flow around a Rotating Circular Cylinder in a Uniform Flow

by

Fumio YOSHINO*, Tsutomu HAYASHI*, Ryoji WAKA*,
Tatsuo HAYASHI*

* Department of Mechanical Engineering

(Received August 2, 1984)

The Navier-Stokes equations were numerically solved on the flow around a rotating circular cylinder in a uniform flow for various rotating speeds at the Reynolds number of 80. The aerodynamic forces on the cylinder, stream lines and vorticity distributions around it were determined.

## 1. Introduction

The history of the research on a rotating cylinder is long. The flow around a rotating cylinder in a uniform flow has been analysed theoretically by Moore[1] and experimented by Tanaka et al.[2] near the transition Reynolds number. Okajima et al.[3] made a research on a circular and an elliptic cylinder vibrating circumferentially in a uniform flow. From these researches, it is seen that the flow pattern around a cylinder changes drastically with the rotating speed. For instance, Okajima et al.[3] found that vortex streets are formed even at the Reynolds number of 40 when the ratio of surface speed of a cylinder to velocity of a uniform flow is 0.2. At this low Reynolds number, the flow is steady and vortex streets are not formed when the cylinder is not rotating. These results, however, are those of analysis of flow at a relatively low rotating speed in a uniform flow, and did reveal neither the mechanism how such a transition occurs nor the interrelation between the rotation of a cylinder and the aerodynamic force on it.

This motivated the authors to calculate a more general case, that is, a flow around a rotating circular cylinder in a uniform shear flow although only the result of a cylinder in a uniform flow is presented here. The finite difference method was made use of to solve the Navier-Stokes equations at a relatively low Reynolds number such as 80.

## 2. Nomenclature

| | |
|---|---|
| $a$ | : radius of the circular cylinder |
| $a_{st}$ | : distance from the center of the cylinder to the stagnation point |
| $C_l$ and $C_d$ | : lift and drag coefficients, respectively |
| $C_{lp}$ and $C_{dp}$ | : pressure components of $C_l$ and $C_d$, respectively |
| $C_{ls}$ and $C_{ds}$ | : shear stress components of $C_l$ and $C_d$, respectively |
| $C_p(\eta)$ and $C_\tau(\eta)$ | : coefficients of pressure and shear stress on the cylinder surface |
| $(r, \theta)$ | : cylindrical coordinates (Fig.1) |
| $S_{tr}$ | : the Strouhal number ( $= 2af/U_c$ ) |
| $T$ and $\Delta T$ | : dimensionless time and time step, respectively |
| $u_\infty$ and $U_c$ | : velocity, and that on x axis, at infinitely far upstream, respectively (Fig.1) |
| $V_0$ | : rotational speed ratio of the cylinder ( = circumferential speed of the cylinder/$U_c$ ) |
| $v_\infty$ | : y component of velocity at infinitely far upstream (Fig.1) |
| $V_\xi$ and $V_\eta$ | : $\xi$ and $\eta$ components of velocity, respectively |
| $(x, y)$ | : rectangular coordinates (Fig.1) |

$\varepsilon$ : dimensionless velocity gradient (vorticity) of the uniform shear flow ( $= a/U_c \, \partial u_\infty / \partial y$ )

$\zeta$ : vorticity

$(\xi, \eta)$ : orthogonal curvilinear coordinates (Fig.1)

$\Psi$ : stream function

The symbols - and $\sim$ on respective items above indicate time mean value and amplitude of periodic fluctuation of a related physical or field quantity, respectively.

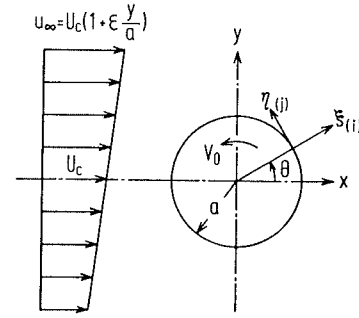


Fig.1 The coordinate systems and nomenclature

## 3. Fundamental Equations and Boundary Conditions

It is assumed that the flow is two-dimensional and incompressible. The coordinate system as indicated in Fig.1 is used to give a magnified view particularly of a complicated flow near the cylinder. The relations of the coordinates $(\xi, \eta)$ to $(r, \theta)$ and $(x, y)$ are as follows;

$$\xi = \log(r/a) \qquad x = ae^{\xi} \cos\eta$$
$$\eta = \theta \qquad y = ae^{\xi} \sin\eta \qquad (1),$$

where the scale factors $h_\xi$ $(=\sqrt{(\partial x/\partial\xi)^2 + (\partial y/\partial\xi)^2})$ and $h_\eta$ $(=\sqrt{(\partial x/\partial\eta)^2 + (\partial y/\partial\eta)^2})$ are such that $h_\xi = h_\eta = h = ae^{\xi}$. The vorticity transport equation and relation of the stream function to vorticity are represented in $(\xi, \eta)$ coordinates, using vorticity, stream function, time, pressure and scale factor nondimensionalized by a and $U_c$ such as

$$\zeta^* = \zeta(a/U_c) \quad , \quad \Psi^* = \Psi/(aU_c) \quad , \quad T^* = T(U_c/a)$$
$$P^* = P/(\rho U_c^2) \quad , \quad h^* = h/a$$

The expressions are as follows;

$$h^2 \frac{\partial\zeta}{\partial T} + \frac{\partial\Psi}{\partial\eta}\frac{\partial\zeta}{\partial\xi} - \frac{\partial\Psi}{\partial\xi}\frac{\partial\zeta}{\partial\eta} = \frac{2}{R_e}\left(\frac{\partial^2\zeta}{\partial\xi^2} + \frac{\partial^2\zeta}{\partial\eta^2}\right) \qquad (2),$$

$$\zeta = -\frac{1}{h^2}\left(\frac{\partial^2\Psi}{\partial\xi^2} + \frac{\partial^2\Psi}{\partial\eta^2}\right) \qquad (3),$$

where $R_e$ is the Reynolds number and the superscript * to show a dimensionless

quantity is dropped for simplicity hereafter.

The no-slip condition on the surface of the cylinder results in the following boundary conditions;

$$V_\xi = \frac{\partial \Psi}{h \partial \eta} = 0 \quad , \quad V_\eta = -\frac{\partial \Psi}{h \partial \xi} = V_0 \tag{4},$$

where the rotational speed ratio $V_0$ is the ratio of circumferential speed of the cylinder to $U_c$. The uniform shear flow infinitely far from the cylinder is expressed as follows;

$$u_\infty = U_c \left( 1 + \varepsilon \frac{y}{a} \right) \quad , \quad v_\infty = 0 \tag{5},$$

where $\varepsilon$ is dimensionless vorticity and means a dimensionless velocity gradient of the uniform shear flow.

## 4. Method of Calculation

### 4.1 Finite difference equations

The domain ( Fig.1 ) was divided into N equal parts in the $\eta$ direction ( subscript j ) starting from the trailing edge of the cylinder and with the interval S ( $= 2\pi/N$ ), equal to that in the $\eta$ direction, in the $\xi$ direction ( subscript i ). A forward difference was used for the time at each grid point while a central difference approximated by the average of the values at the times T and $T + \Delta T$ being used for ( $\xi$ , $\eta$ ) coordinates. The finite difference approximations of Eqs.(2) and (3) are as follows;

$$\begin{aligned}
&\frac{h^2}{\Delta T} \left( \zeta_{i,j}^{T+\Delta T} - \zeta_{i,j}^{T} \right) = \\
&= \frac{1}{R_e S^2} \{ ( \zeta_{i+1,j} + \zeta_{i-1,j} + \zeta_{i,j+1} + \zeta_{i,j-1} - 4\zeta_{i,j} )^{T} + \\
&+ ( \zeta_{i+1,j} + \zeta_{i-1,j} + \zeta_{i,j+1} + \zeta_{i,j-1} - 4\zeta_{i,j} )^{T+\Delta T} \} + \\
&+ \frac{1}{8S^2} [ \{ ( \Psi_{i+1,j} - \Psi_{i-1,j} )^{T} ( \zeta_{i,j+1} - \zeta_{i,j-1} )^{T} + \\
&+ ( \Psi_{i+1,j} - \Psi_{i-1,j} )^{T+\Delta T} ( \zeta_{i,j+1} - \zeta_{i,j-1} )^{T+\Delta T} \} - \\
&- \{ ( \Psi_{i,j+1} - \Psi_{i,j-1} )^{T} ( \zeta_{i+1,j} - \zeta_{i-1,j} )^{T} + \\
&+ ( \Psi_{i,j+1} - \Psi_{i,j-1} )^{T+\Delta T} ( \zeta_{i+1,j} - \zeta_{i-1,j} )^{T+\Delta T} \} ]
\end{aligned} \tag{6},$$

$$\Psi = \Psi_p + \hat{\Psi} \quad , \quad \Psi_p = ( e^{\xi} - 1/e^{\xi} ) \sin \eta$$

$$\Psi^{m+1}_{i,j} = \Psi^{m}_{i,j} + \frac{\alpha_\Psi}{4}(\Psi^{m}_{i+1,j} + \Psi^{m+1}_{i-1,j} + \Psi^{m}_{i,j+1} + \Psi^{m+1}_{i,j-1} - 4\Psi^{m}_{i,j} + S^2 h^2_{i,j}\zeta^{T+\Delta T}_{i,j}) \quad (7),$$

where $\alpha_\Psi$ is a relaxation factor and m is number of iterations.

The boundary conditions on the surface of the cylinder are approximated by

$$\Psi_{1,j} = 0$$

$$\zeta_{1,j} = -\frac{3}{S^2 h^2_{1,j}}(\Psi_{2,j} - \Psi_{1,j} + V_0 h_{1,j} S) - \frac{\zeta_{2,j}}{2}\left(\frac{h_{2,j}}{h_{1,j}}\right)^2 \quad (8),$$

considering Eq.(4)[3]. Although there exists a problem such as determining a level of the stream function since the equations in infinite domain are numerically solved in finite domain, the value of $\Psi$ on the surface of the cylinder is made equal to zero. This will not introduce any large error since the domain of calculation is taken wide enough as $r_\infty > 100a$. Then Eq.(5) for the outer boundary of this domain results in the following relations;

$$\Psi_{\infty,j} = e^{\xi_\infty}\sin\eta_j + \frac{\varepsilon}{4}e^{2\xi_\infty}(1 - \cos 2\eta_j)$$

$$\zeta_{\infty,j} = -\varepsilon \quad (9).$$

Two kinds of initial values were used in order to solve Eqs. (6) and (7) under the boundary conditions (8) and (9). The inviscid solution[4] of the flow around a still cylinder in a uniform shear flow, i.e.,

$$\Psi_{i,j} = \left(e^{\xi} - \frac{1}{e^{\xi}}\right)\sin\eta + \frac{\varepsilon}{4}\left\{e^{2\xi}(1 - \cos 2\eta) + \frac{\cos 2\eta}{e^{2\xi}} - 1\right\}$$

$$\zeta_{i,j} = -\varepsilon \quad (10)$$

was employed as the initial value of the case of $\varepsilon \neq 0$ and $V_0 \neq 0$. In the case of $\varepsilon = 0$ and $V_0 \neq 0$, the result of computation at $V_0$ was employed as the initial value for the computation of the next larger $V_0$. The result of computation was concluded to have converged when the residuals of iteration of respective $\Psi$ and $\zeta$ at a time T became less than $\pm 1\%$ and $\pm 5\%$ of $S^3$, respectively.

4.2 Aerodynamic and stress coefficients

The solutions $\Psi$ and $\zeta$ at a time T obtained by iterative computation can be used to calculate the pressure and shear stress distributions on the surface of the cylinder. Rewriting the fundamental equations by making use of Eqs.(4) on the surface yields the relative pressure at a point of $\eta$ to that at the trailing edge of the cylinder ($\eta = 0$) in a dimensionless form (divided by $\rho U_c^2/2$),

$$C_p(\eta) - C_p(0) = \frac{4}{R_e}\int_0^\eta \left(\frac{\partial\zeta}{\partial\xi}\right)_{\xi=0} d\eta \quad (11).$$

The shear stress is easily obtained to give

$$C_\tau(\eta) = \frac{4}{R_e}\left(\frac{\partial V_\eta}{h\partial\xi} - \frac{V_\eta}{h}\right) \qquad (12).$$

The condition that Eq.(11) should give zero at $\eta = 2\pi$ is not always satisfied[5] in real computation due to an error in the calculation. Hence, the pressures at $\eta = \pm 2\pi$ were averaged to give the value at $\eta = 0$.

The pressure ( subscript p ) and shear stress ( subscript s ) components of the lift and drag coefficients ($C_l$ and $C_d$, respectively) are obtained from the following integration;

$$C_{lp} = -\frac{1}{2}\oint C_p(\eta)\sin\eta\, d\eta \quad , \quad C_{dp} = -\frac{1}{2}\oint C_p(\eta)\cos\eta\, d\eta$$

$$C_{ls} = \frac{1}{2}\oint C_\tau(\eta)\cos\eta\, d\eta \quad , \quad C_{ds} = -\frac{1}{2}\oint C_\tau(\eta)\sin\eta\, d\eta$$

$$C_l = C_{lp} + C_{ls} \quad , \quad C_d = C_{dp} + C_{ds} \qquad (13).$$

The definition of the Strouhal number $S_{tr}$ is as follows;

$$S_{tr} = \frac{2af}{U_c} \qquad (14),$$

where f is the frequency of the fluctuating lift.

The computation was made using M-200 of Data Processing Center of Kyoto University.

## 5. Results and Discussion

Figure 2 compares the relation of the drag coefficient to the Reynolds number of a still cylinder in a uniform flow, obtained by the present calculation, with the results of calculation and experiment by the other researchers. The values of the parameters used for the present computation are as follows: $S=2\pi/40$, $\Delta T=0.01$, $\alpha_\psi=1.84$, $r_\infty \fallingdotseq 95a$ when $R_e = 20$ and $S = 2\pi/60$, $\Delta T = 0.05$, $\alpha_\psi = 1.60$, $r_\infty \fallingdotseq 111.3a$, $T \leqq 100.0$ when $R_e = 80$. The figure shows a good agreement of the present calculation with those by the others[3],[5],[6] which implies that the present calculation can well be applied

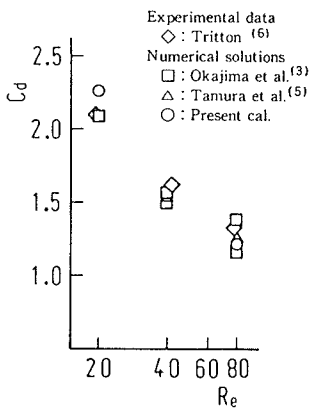


Fig.2 Dependency of drag coefficient on the Reynolds number

to the case of a rotating cylinder in uniform and uniform shear flows. The following computations were made with the values of the parameters given above at $R_e = 80$.

Figures 3 and 4 show the time-dependent lift and drag coefficients, respectively, of the rotating cylinder in a uniform flow, in which the rotational speed ratio $V_0$ was changed from 0 to -5.5. That $V_0<0$ indicates that the cylinder rotates in the counter arrow direction of Fig.1. The figure shows that values of $C_l$ and $C_d$ attain those of a stationary state for $T > 50$, from which the time mean values $\bar{C}_l$ and $\bar{C}_d$ are the averages of $C_l$ and $C_d$ for $T > 50$, respectively. Figure 3 indicates that value of $\bar{C}_l$ increases with $|V_0|$ and reaches a maximum of about 6.8 at $V_0 = -4$. The amplitude of the periodic fluctuation is too small to distinguish from the T axis when $V_0=0$ though $C_l$ surely fluctuates periodically at this $V_0$, increases with $|V_0|$, and becomes larger at $V_0 = -1$ than 10 times that at $V_0 = 0$. The fluctuation, however, dampens with a further increase of $|V_0|$, and dies out for $|V_0| \geq 2$, which implies that there can exist a steady flow when $|V_0|$ is large even at such a Reynolds number of 80 that Kármán's vortex street is formed behind a still cylinder. As shown in Fig.4, the value of $\bar{C}_d$ too increases with $|V_0|$, and the rate of increase is particularly large near $V_0$

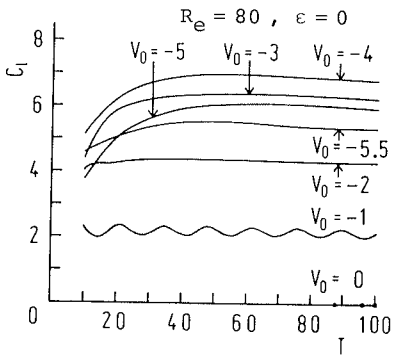


Fig.3 Variation of lift coefficient with time

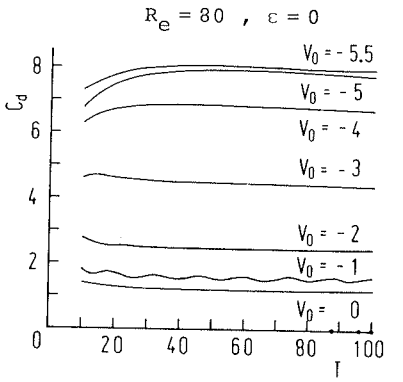


Fig.4 Variation of drag coefficient with time

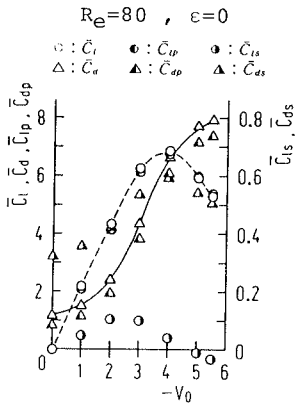


Fig.5 Relation of lift and drag coefficients to rotational speed ratio

$= -3$. The amplitude of the fluctuation of $C_d$ has the same tendency as that of $C_l$, but is smaller. Figure 5 indicates $\overline{C}_l$, $\overline{C}_d$ together with the pressure and shear stress components of them against $V_0$, and confirms what was mentioned above about $\overline{C}_l$ and $\overline{C}_d$. The figure also indicates that the pressure components $\overline{C}_{lp}$ and $\overline{C}_{dp}$ account, broadly speaking, for 90% of $\overline{C}_l$ and $\overline{C}_d$, respectively, at any $V_0$.

The stream lines and equi-vorticity lines in the flow field are shown in Figs.6 and 7, respectively. The figures (a) and (b) correspond to the cases of ($V_0 = -1$, $T = 96.0$) and ($V_0 = -4$), respectively. The value of $C_l$ is about minimum when $T = 96.0$ at $V_0 = -1$ (Figs.(a)). Figure 6 shows that the wake deflects downwards of the figure as $|V_0|$ increases. This downward deflection is considered to be due to the fact that the total vorticity in the wake becomes positive by addition of positive vorticity generated by the rotation of the cylinder. For example, the positive vorticity near the lower surface of the cylinder is carried toward the upper side, in the rotational direction and into the wake by convection and diffusion ( Figs.7(a) and (b)). The vorticity is in fact positive anywhere in the wake at $V_0 = -4$. This positive vorticity in the wake induces a downward velocity which in turn deflects the wake downwards and gen-

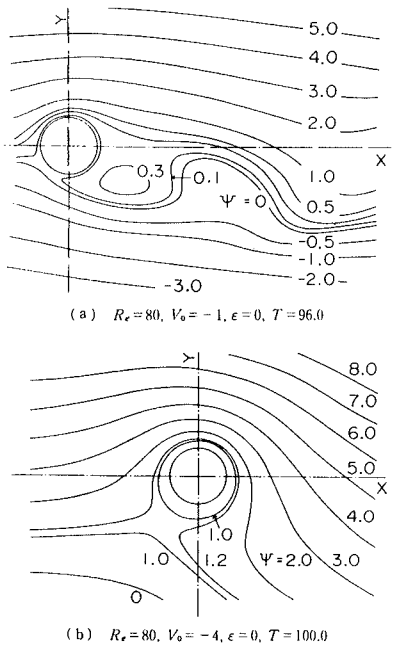


Fig.6 Stream lines around the rotating cylinder

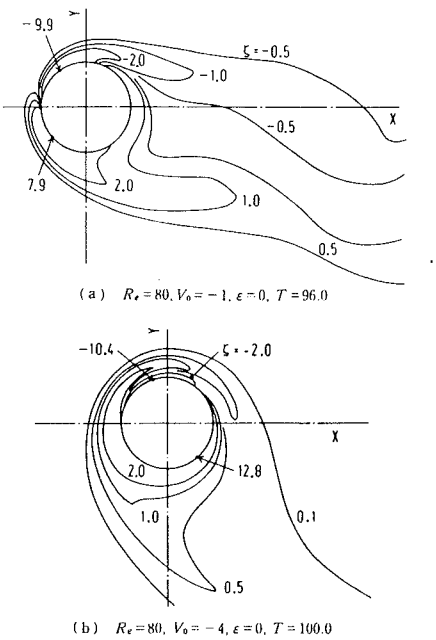


Fig.7 Equi-vorticity lines around the rotating cylinder

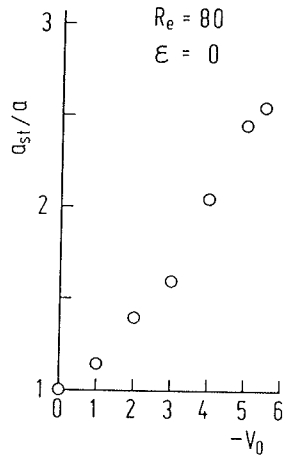


Fig.8 Distance from the stagnation point to the center of the cylinder

erates an induced drag on the cylinder to increase $\bar{C}_d$ with $|V_0|$ (different in origin from that of a finite span wing). That is, the increase of $\bar{C}_d$ with $|V_0|$ is considered to be mainly due to the increase of induced drag. The increase of $\bar{C}_d$ with $|V_0|$ is observed in the case of a cylinder rotating at a relatively higher speed in a high Reynolds number flow.[2] Figure 8 indicates the distance to the upstream stagnation point from the center of the cylinder obtained from stream line distribution. The stagnation point is not on the surface of the cylinder when $V_0 \neq 0$ and moves farther away from the cylinder as $|V_0|$ increases. The angular position of the point stays near $\theta \fallingdotseq 220°$ irrespective of $V_0$ as seen from Figs.6(a) and (b), which is considered to be due to cancellation of the change of $\theta$ due to the increase of circulation with $|V_0|$ by that due to the increase of intensity of downwash.

## 6. Conclusions

Numerical solutions for $R_e = 80$ were obtained on the flows around a circular cylinder with the rotational speed ratio $V_0$ of $0 \sim -5.5$ in a uniform flow ($\varepsilon = 0$). The following are conclusions.

(1) $\bar{C}_l$ increases with $|V_0|$, reaches a maximum ($\fallingdotseq 6.8$) at $V_0 = -4$, and decreases thereafter. $\bar{C}_d$ increases with $|V_0|$. The pressure components $\bar{C}_{lp}$ and $\bar{C}_{dp}$ account for most of $\bar{C}_l$ and $\bar{C}_d$, respectively.

(2) $\tilde{C}_l$ reaches a maximum for $|V_0| < 2$, and is nearly zero for $|V_0| \geqq 2$. $\tilde{C}_d$ shows the same tendency as $\tilde{C}_l$ though the former is smaller than the latter.

(3) The wake deflects downwards due to the rotation ($V_0 < 0$) of the cylinder, that is, due to the induced velocity in such a way that the deflection is larger when $|V_0|$ is larger. The stagnation point moves away from the cylinder as $|V_0|$ increases. The angular position of the point approaches, first, rapidly $\theta \fallingdotseq 220°$, but stays about there even if $|V_0|$ increases further.

## References

(1) Moore, D.W., J. Fluid Mech., Vol.2,No.6 (1957-8), p.541.

(2) Tanaka, H. and Nagano, S., Trans. Japan Soc. Mech. Engrs. (in Japanese);

Vol.38, No.310 (1972-6), p.1343.

(3) Okajima, A., et al., Trans. Japan Soc. Mech. Engrs. (in Japanese), Vol.37, No.304 (1971-12), p.2300.

(4) Frenkiel, F.N. and Temple, G.(ed.), Applid Mathematics and Mechanics, Vol.8 (1964), p.12, Academic press.

(5) Tamura, H., et al., Trans. Japan Soc. Mech. Engrs. (in Japanese), Vol.46, No.404 (1980-4), p.555.

(6) Tritton, D.J., J. Fluid Mech., Vol.6, No.4 (1954-11), p.547.